RSC Advances

ROYAL SOCIETY OF CHEMISTRY

www.rsc.org/advances

RSC Advance

ARTICLE

Synthesis of pure nickel(III) oxide nanoparticles at room temperature for Cr(VI) ion removal

ngtarReceived 00th January 20xx,
Accepted 00th January 20xx

DOI: 10.1039/x0xx00000x

www.rsc.org/

Sayan Dey[(a)], Swarupananda Bhattacharjee[(a)], Mahua Ghosh Chaudhuri[(a)], Raj Shekhar Bose[(b)], SumanHalder[(c)] and Chandan Kr. Ghosh[(a),*]

Ni_2O_3 nanoparticles of various size (~ 25.8 to 49.7 nm), obtained by a facile oxidation process using $Ni(NO_3)_2.6H_2O$, NaOH and sodium hypochlorite as precursor materials at various temperatures (0^o, 25^o, 50^o and 70^oC), is found to remove toxic Cr(VI) from aqueous solution (20 g L^{-1}). The structural, morphological, surface charge and chemical compositions of the synthesized samples were characterized by XRD, TEM, zeta potential and EDX respectively. Adsorption capacity is found to be strongly dependent on the size and surface heterogeneity of the synthesized particles and the plausible mechanism for such significant adsorption efficacy is attributed to the sorbate – sorbent electrostatic interaction and shielding of Cr(VI) ions. The adsorption mechanism fits with the Langmuir isotherm model with maximum 60% Cr(VI) removal capacity (20.768 mg g^{-1} (calculated) and 20.408 mg g^{-1} (predicted from isotherms)) corresponding to Ni_2O_3 nanoparticles, prepared at 70^0C in 3 hours at room temperature. Thermodynamic parameters, obtained from fitting, demonstrate that the adsorption process being endothermic in nature follow pseudo-second-order kinetic model. The spontaneity of the adsorption process gets reduced with increasing particle size. pH of the solution is observed to have a remarkable effect on the adsorption, giving maximum adsorption at pH = 6.

Introduction

The presence of various heavy metals like Cr(VI), As(III), U(VI) etc. in aquatic environment causes major concern for aquatic life, human health due to their severe toxicity.[1] Among them, Cr(VI) though exists in the effluents of various industries like electroplating, pigments etc. and is identified to be one of the most fatal species due to their carcinogenic effects on human beings and their abundance in drinking water.[2]Out of two different form of chromium, hexavalent (Cr(VI)) and trivalent form (Cr(III)) in aqueous medium, Cr(III) precipitates in its hydroxide and oxide forms, therefore they don't migrate in the solution and are easily separable. On the other hand, Cr(VI) being highly soluble in water is observed to be highly toxic due to its high redox potential and causes cancer, kidney damage, gastrointestinal disorder etc.[3,4]In this context, it may be stated that US Environmental Protection Agency (EPA) and World Health Organization (WHO) have set maximum allowed level of Cr(VI) concentration in drinking water 100 μgL^{-1} and 50 μgL^{-1} respectively.[5]Till date, among different readily available methods like chemical precipitation, solvent extraction, membrane separation, ion exchange, adsorption etc. to remove Cr(VI), adsorption is found to be the most suited one that is being successfully used to remove from its respective aqueous solutions.[6, 7]The most

[(a)]*School of Materials Science and Nanotechnology, Jadavpur University, Kolkata-700032, India*
[(b)]*School of Environmental Studies, Jadavpur University, Kolkata – 700032, India.*
[(c)]*Department of Pharmaceutical Technology, Jadavpur University, Kolkata – 700032, India*
* *Corresponding author's e-mail ID: chandu_ju@yahoo.co.in*

commercially used material for this purpose is the activated carbon or mesoporous carbon due to their high surface porosity.[8, 9] Apart from them, bio-adsorbents are often used as adsorbents in waste water treatment.[10–13] However, they have weak mechanical strength, poor separation capacity and hence they are not very effective in this field. Recently, alternative materials including various oxide based nanocomposites and nanostructure have been synthesized as potential adsorbent of heavy metal ions.[14,15] Thus, with the advancement of technology, newer materials with improved adsorption capacities are being developed. In this context, it has to be mentioned that metal oxides are known to have high adsorption capacity of toxic metals in nano-dimensions. Iron and aluminium oxide have been identified to adsorb toxic substances from waste water effectively due to their high surface adsorption ability.[16-18] Among different transitional materials, developed so far, NiO has proven itself as an another promising material that shows potential application in battery electrodes, super-capacitors, smart windows, catalysis etc.[19-22] Nickel, being a transitional metal, possesses variable oxidation states, but most of them are found to be abundant in normal conditions.[23, 24] In this context, it has to be mentioned that pseudo hydrate of Ni(III) oxide was reported but their anhydrous form was not observed due to easy transformation of them into NiO on heating.[25] On the other hand, it was established that these higher oxides may possess many interesting properties if obtained in anhydrous form.

According to the reviewed literature, the preparation of the pure Ni(III) oxide (Ni_2O_3) was not feasible by standard synthesis procedures like sol gel, hydrothermal, solvothermal etc. No systematic study was performed on this material so far.In this study, wehave successfully prepared pure $Ni_2O_3$by an environment friendly, facile, chemical precipitation method at room temperature. The synthesis was carried out in a range of temperature to study the size effect on its Cr(VI) removal efficiency from waste water.

Experimental

Preparation of pure Ni_2O_3 nanoparticles

All the reagents were procured from MERCK India Pvt. Ltd. and were used without further purification. Pure Ni_2O_3 nanoparticles were synthesized by sustained oxidation of nickel precursors. In a typical experiment, 1.00 g of $Ni(NO_3)_2.6H_2O$ was dissolved in 20 ml deionized water under constant stirring. In another beaker, 1.60 gm NaOH was dissolved in 15 ml of sodium hypochlorite solution having 4% active chlorine. The alkaline solution of hypochlorite was added dropwise under constant stirring to the solution containing nickel precursor. The stirring was continued for half an hour to obtain black precipitate that formed as flocculates almost immediately after adding the hypochlorite solution. The precipitate was collected by filtration and dried to form grayish black powder of hydrated nickel (III) oxide ($Ni_2O_3.xH_2O$). This powder was then treated with 20 ml sodium hypochlorite solution under constant stirring for an hour to form a suspension. The suspension was left idle till the effervescence ceases and a dark black precipitate forms at the bottom of the beaker. This precipitate was then further washed with a small amount of hypochlorite solution, centrifuged at 20,000 rpm, collected and dried over hot air oven to obtain crystals of pure Ni(III) oxide nanoparticles. In order to investigate the temperature effect on particle size, the synthesis reaction was carried out at four different temperatures viz. freezing temperature (0^oC), Room Temperature (RT) (25^oC), 50^oC and 70^oC respectively.

Characterization

Crystallinity and phase purity of the synthesized samples were investigated by Ultima-III, Rigaku x-ray diffractometer (Cu K_α radiation, λ = 1.5404 Å). Chemical analysis of the synthesized samples were carried out using energy dispersive attached with field emission scanning electron microscope (S – 4800, Hitachi). Transmission electron microscope (TEM, JEM – 2100,

JEOL)was used to investigate the microstructure and morphology of the synthesized samples. Surface potential was measured using Zetasizer NS Nano.

Adsorption of Cr(VI) by pure Ni_2O_3 nanoparticles

A batch adsorption procedure was applied to study the sorption of Cr(VI) ions by Ni_2O_3 nano-particles as proposed by Yao et. al.[26]Dichromate stock solution was prepared by dissolving 0.40 gm of $K_2Cr_2O_7$ in 20 ml of deionized water. 20.00 mg of the powdered Ni_2O_3sample was dispersed into the stock solution under constant stirring at room temperature. In order to investigate the effect of contact time,adsorption kinetics, adsorption process was carried out at seven different time intervals viz. 15 minutes, 30 minutes, 45 minutes, 1 hour, 1.5 hours, 2 hours and 3 hours. Each solution was centrifuged twice at 20,000 rpm for 10 minutes to remove any Ni_2O_3 particle and the residual solution was collected in glass vials for further analysis. Amount of adsorbed chromium was calculated using standard calibration curve as proposed by Ansari et. al.[11]Pure Ni_2O_3 particles were collected after centrifugation to investigate any change in phase. It has been found that the crystal structure of the particles after the adsorption remains unchanged. The liquid samples collected after adsorption is subjected to serial dilution procedure to 10^{-4}M for ultraviolet spectroscopy between 800 nm and 200 nm (Perkin Elmer). After determining initial and final concentrations of the solution, adsorption percentage and adsorption capacity (Q_e) were calculated using the relations in equations (1) and (2):[10]

$$\text{Adsorption } \% = \frac{C_o - C_e}{C_o} \times 100 \qquad (1)$$

and

$$Q_e = \frac{(C_o - C_e).V}{m} \qquad (2)$$

where $C_o$and $C_e$represent the initial and final concentration of Cr(VI) in g/L. 'V'and 'm' are the volume of the testing solution (in ml) and mass of the sorbent (in mg) respectively.

Results and Discussion

Crystal structure determination by x-ray diffraction

The x-ray diffraction pattern of the pure dried powder samples are represented in Figure 1. Diffraction peaks, obtained at 27.34°, 31.66°, 45.41°, 56.38°and 66.12°are readily be indexed with (101), (002), (111), (202) and (004) plane of hexagonal Ni_2O_3(JCPDS Card Number 14-0481, CAS Number 1314-06-3). Absence of any peak other than Ni_2O_3 rules out the presence of any impurity phase and confirms the phase purity of Ni_2O_3.

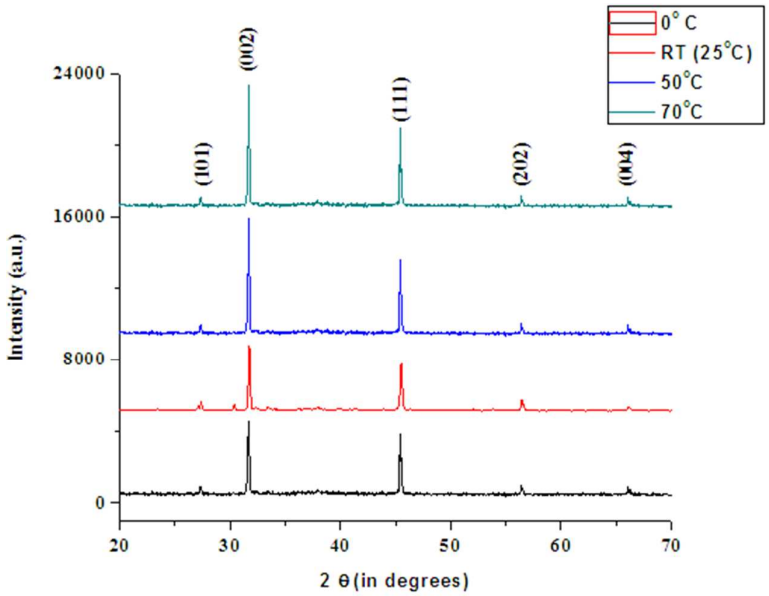

Figure 1: X-ray Diffraction pattern of pure Ni_2O_3 nanoparticles

The particle sizes of the synthesized samples, calculated using the Scherrer's formula.[27] are listed in Table 1. It is noticed that the particle size increases on increasing the synthesis temperature.

Table 1: Particle sizes of Ni_2O_3 nanoparticles based on the synthesis temperatures

Temperature of Synthesis	Particle Size (in nm)
0°C	25.8
RT (25°C)	34.2
50°C	42.6
70°C	49.7

Equation (3) that represents the variation of particles size with synthesized temperature can be used to calculate the activation energy (E_a) of formation of pure Ni_2O_3 nanoparticles.[28]

$$r = r_0 e^{\frac{-E_a}{kT}} \quad (3)$$

where,'r' and 'k' represent the size of the particle synthesized at absolute temperature 'T' and Boltzmann's constant respectively. From slope of the lnr vs. 1/T curve(shown in Figure 2), E_a is calculated to be ~75.49 meV.

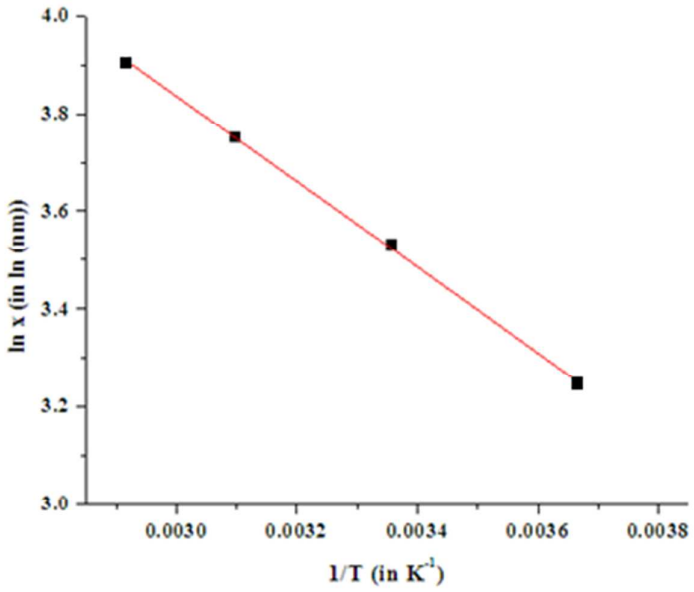

Figure 2: Arrhenius plot for calculation of the activation energy of formation of pure Ni_2O_3 nanoparticles

Synthesis mechanism of pure Ni_2O_3nanoparticles

Synthesis of pure Ni_2O_3 involves a rapid competitive oxidation of the nickel precursor. The whole reaction may be sub-divided into two broad divisions viz, active chlorination of the nickel precursor resulting in the preferential active oxygen attachment to the nickel ion that results in the formation of hydrated nickel(III) oxide in water medium and basic pH. The second step involves forced and prolonged oxidation of the so formed hydrated oxide to form pure anhydrous Ni_2O_3 nanoparticles. The detailed steps may be predicted as follows:

Firstly, dissociation of nickel precursor($Ni(NO_3)_2.6H_2O$) takes place into Ni^{2+} and NO_3^- ions in the presence of water. A standard alkaline solution of sodium hypochlorite (having 4% active chlorine) that is introduced to the prepared solution acts as a source of active oxygen. In presence of H^+ ions (which is present in the solution in abundance), NaOCl dissociates to form one nascent oxygen and HCl. The alkaline solution of NaOCl (as used in this experiment) neutralizes the so formed HCl and prevents the formation of $NiCl_2$ as an unwanted product.

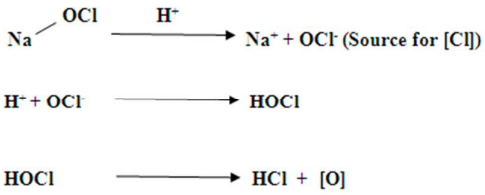

The nascent oxygen, also known as reactive oxygen having one lone electron, would try to acquire one more electron to stabilize its atomic configuration. As the nascent oxygen is formed within the solution, it readily oxidizes the Ni^{2+} species by accepting one electron from the ions to form Ni^{3+} ions. The ionic reaction can be written as below.

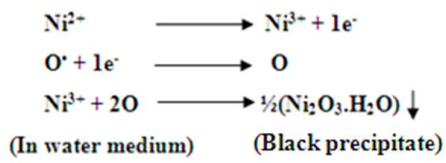

Nickel ions, seated above H^+ and Na^+ in the electrochemical series, preferentially gets oxidized by the [O] or $O^{\bullet}$ species present in the solution. Thus, after this reaction, a pseudo hydrated oxide of trivalent nickel is formed. This is due to the competitive attachment of [O] and OH^- to the nickel cation. The detailed ion movement is schematically shown below:

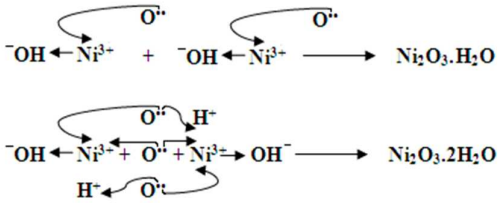

The second step involves forced and prolonged oxidation of the Ni–OH bonds so formed to convert it to Ni=O thereby forming anhydrous Ni_2O_3. The detailed mechanism is shown below:

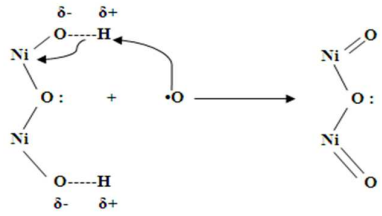

The nascent oxygen attacks the slight positive charge centre of H^+ to remove it from the hydrated structure. This results the formation of the unstable dangling bond due to the cleavage of the O-H bond which immediately stabilizes by forming a double bond with nickel. Same mechanism is followed by the other Ni - OH bonds. As a result, pure Ni_2O_3 phase is obtained. In order to identify the ratio of Ni:O, chemical analysis using EDAX spectroscopy was carried out and the analysis shows the ratio to be 2:3(Figure S – 1 in ESI).

Figure 3(a) and (b) represent the transmission electron microscope (TEM) images that reveal uniform distribution of particles. A histogram for the particle size distribution, represented in the inset of Figure 3(a), indicates the narrow size distribution of the particles.

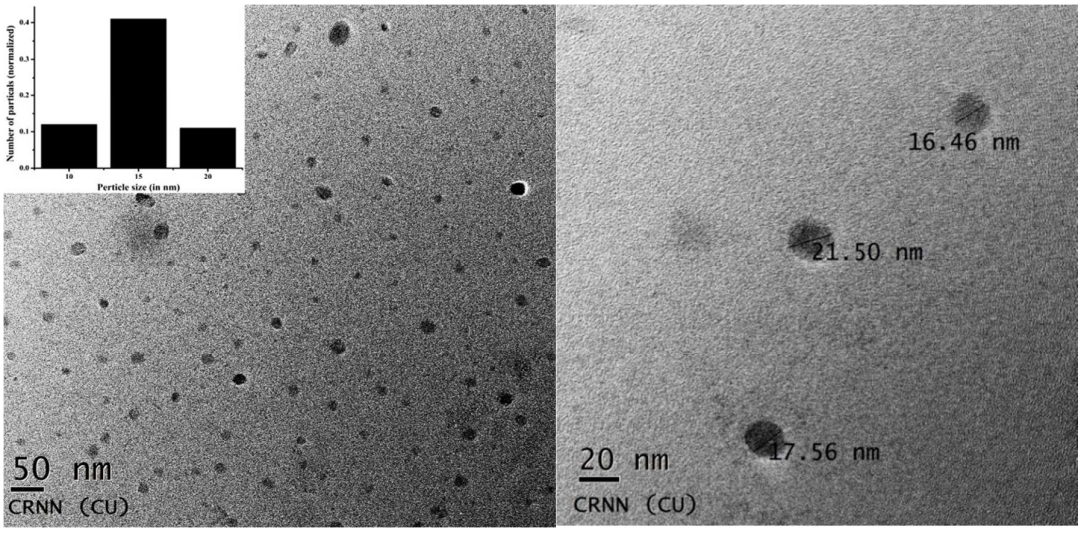

(a) (b)

Figure 3: (a) TEM micrograph of pure Ni_2O_3 nanoparticles showing particle size distribution (b) TEM micrograph of pure Ni_2O_3 nanoparticles showing particle size

Removal of Cr(VI) ions from aqueous solution

The batch experiments for Cr(VI) ion removal were carried out for Ni_2O_3corresponding to four different particle size as performed by Liu et.al.[14]The temperature (25^oC), pH (~6) and concentration of $Cr_2O_7^{2-}$ and $Ni_2O_3$of the solution were kept constant. When Cr(VI) is absorbed as chromate i.e. in alkaline medium, it possesses a peak in the range of 460 nm to 340 nm. The amount of removed Cr(VI) was calculated using the standard calibration curve obtained for spectrophotometric determination of Cr(VI).[29] It was found that Cr(VI)removal efficiency is different for samples having different particle size.Cr(VI) removal capabilities of the synthesized nanoparticles was examined with respect to volume of the stock solution, pH of the solution, adsorbent dose, adsorbate dose, shaker speed and are discussed in the ESI.

Mechanism of Cr(VI) ions adsorption from aqueous solution

To understand the basic mechanism of Cr(VI) removal, it is essential to study the behaviour of the adsorbate and the adsorbant in presence of a polar solvent (in this case, water). In acidic medium having pH < 6, Cr(VI) exists as $HCrO_4^-$ while in neutral pH, it exists as CrO_4^- (chromate ion). The chromate ion possesses tetrahedral geometry with partial positive chromium centre surrounded by four oxygen atoms having two lone pairs that stabilize the structure.The experiment was carried out close to the neutral pH where the chromate ions are predominant.[2] Chromate ions, due to the presence of two lone pairs, attract the positive species towards itself thereby making the Cr(VI) more positive. Thus, eventually, Cr(VI) becomes loosely bound to its surrounding oxygen. Ni_2O_3 on the other hand, has a lone pair of electron and four bonded pairs of electrons. This lone pair of electron acts as a negative charge centre. This negative centre attracts the δ+ Cr(VI) centre of the loosely bonded chromate ion towards the particle surface. This leads to the adsorption of the Cr(VI) ion onto the particle surface. Each particle can pick up one Cr(VI) molecule at a time. However, from Figure 4, it is found that close to about 60% Cr(VI) ions are removed from the solution. Weight percent of Cr in $K_2Cr_2O_7$ is ~33% of the total weight of the molecule. So, out of 400.00 mg $K_2Cr_2O_7$ used for the experiment, only 132.00 mg Cr is available for active adsorption. 20.00 mg adsorbant can take up 20.00 mg of Cr(VI). The adsorption of the rest ~50.00 mg Cr(VI) corresponding to the highest adsorption result may be attributed to the surface heterogeneity and cationic vacancies on the surface that leads to the formation of more active centers for adsorption of Cr(VI).

Effect of contact time on Cr(VI) adsorption by Ni_2O_3 nanoparticles

The adsorption of Cr(VI) from solution onto pure Ni_2O_3nanoparticles is found to be highly time dependent. It has been observed that the effective adsorption of Cr(VI) ions increases with increase in contact time. The adsorption percentages (adsorption spectra are shown in ESI, Figure S - 7–S - 10), calculated using equation (1), are plotted with respect to the contact time for the four different particles (shown in Figure 4). It can be inferred that maximum Cr(VI) ion adsorption percentage of ~59.62% is achieved by the particles prepared at 70^oC while the others are below 50%.

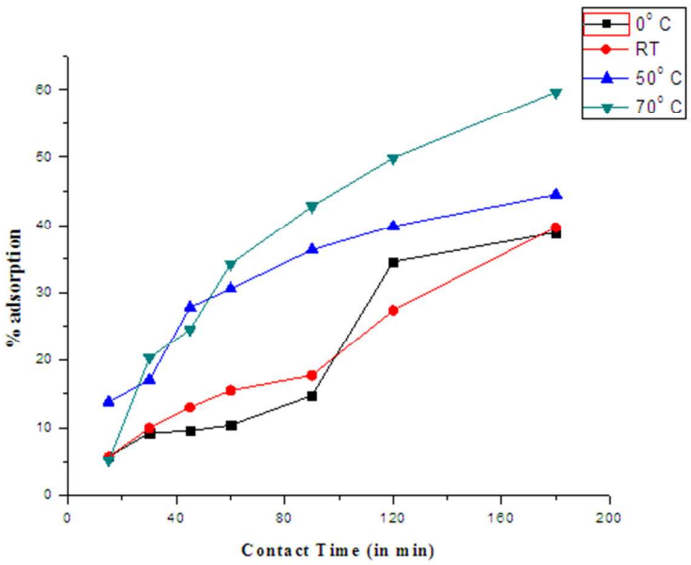

Figure 4: Variation of adsorption percentage with respect to contact time for the particles prepared at different temperatures

The zeta potential measurement reveals that the surfaces of Ni_2O_3 nanoparticles are negativelycharged(Table - 2)that provides ease adsorption of the positively charged metal ions on the surface of the particles.Cr(VI) ions being positively charged are attracted towards a negatively charged surface and effectively get adsorbed. The surface charge developed due to the dispersion of nanoparticles in a solution may be another important factor governing the adsorption. Spectra are presented in the electronic supplementary information (Figure S – 11).

Table 2: Zeta potential of pure Ni_2O_3 nanoparticles

Particle preparation temperature	Zeta Potential (in mV)
0^oC	-26.6
RT (25^oC)	-20.8
50^oC	-21.2
70^oC	-20.1

From table 2, it is observed that all the four particles have a negative surface charge. The smallest particle possesses the highest negative charge followed by the particles prepared at 50^oC which in turn follows the particles prepared respectively at room temperature and 70^oC. Thus, initially, adsorption is high in case of the particles prepared at 0^oC and 50^oC that is evident from Figure 4.Smaller particles having more surface area possesses high shielding effect due to same concentration of H^+ ions in the solution. Therefore, due to less shielding effect by H^+ ions for particles with largest size show the highest Cr(VI) adsorption ability.[30]Figure 5 shows schematically the probable difference in shielding density of H^+ ions in case of two particles of different size.

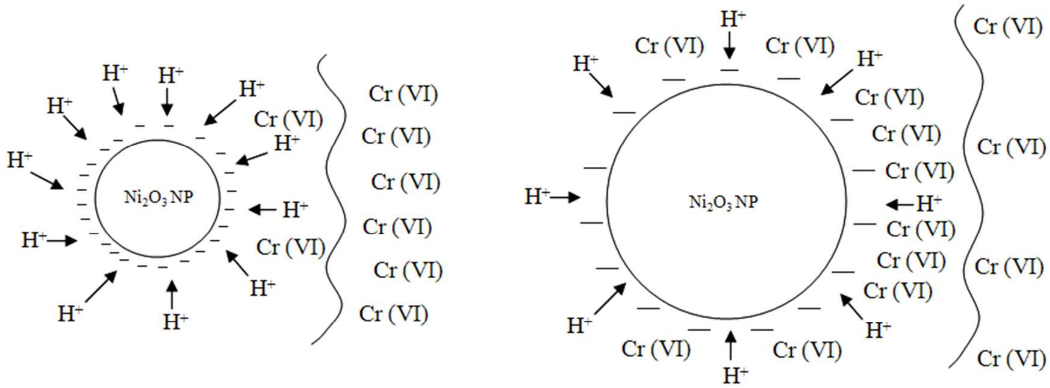

Figure 5: Comparison of shielding effect for particles of different size

Kinetics of Cr(VI) adsorption by pure Ni_2O_3 nanoparticles

In order to understand the appropriate kinetic modelsfor sorption of Cr(IV), the experimentally obtained data of Cr(VI) removal process were simulated using pseudo first order and pseudo second order kinetic model.Pseudo first order model (shown in Figure 6) that often describes the sorption processis expressed as follows:

$$\ln(q_e - q_t) = \ln q_e - k_1 t \qquad (4)$$

The pseudo second order kinetic model (Figure 7) that relates the whole sorption process including sorption and internal particle diffusion and can be written as:

$$\frac{t}{q_t} = \frac{1}{k_2 q_e^2} + \frac{t}{q_e} \qquad (5)$$

where, q_e and q_t are the sorption amounts (mg g^{-1}) at equilibrium time and at time't' respectively; k_1 (min^{-1}) and k_2 (g mg^{-1} min^{-1}) represent the kinetic rate constants corresponding to pseudo-first-order and pseudo-second-order respectively.[30] Obtained kinetic parameters are listed in Table 3. It is observed from the r^2 values that the sorption of Cr(VI) by pure Ni_2O_3 nanocrystals follows the pseudo second order kinetic model. Moreover, the value of q_e, calculated from the second order kinetic model, matches well with its experimental value. This also implies that the absorption is dominated by chemisorption or strong surface complexation rather than mass transport.[31]

Table 2: Kinetics result for adsorption of Cr(VI) by pure Ni_2O_3 nanoparticles

Synthesis temperature (in ^{o}C)	Pseudo First Order Model			Pseudo Second Order Model		
	k_1 (min^{-1})	q_e (mgg^{-1})	r^2	k_2 (g mg^{-1} min^{-1})	q_e (mg g^{-1})	r^2
0^{o}C	0.011	13.90	0.899	0.087	3.35	0.860
25^{o}C (RT)	0.01	14.21	0.8995	0.056	5.38	0.989
50^{o}C	0.006	5.95	0.705	0.042	9.90	0.977
70^{o}C	0.011	8.80	0.569	0.018	20.00	0.973

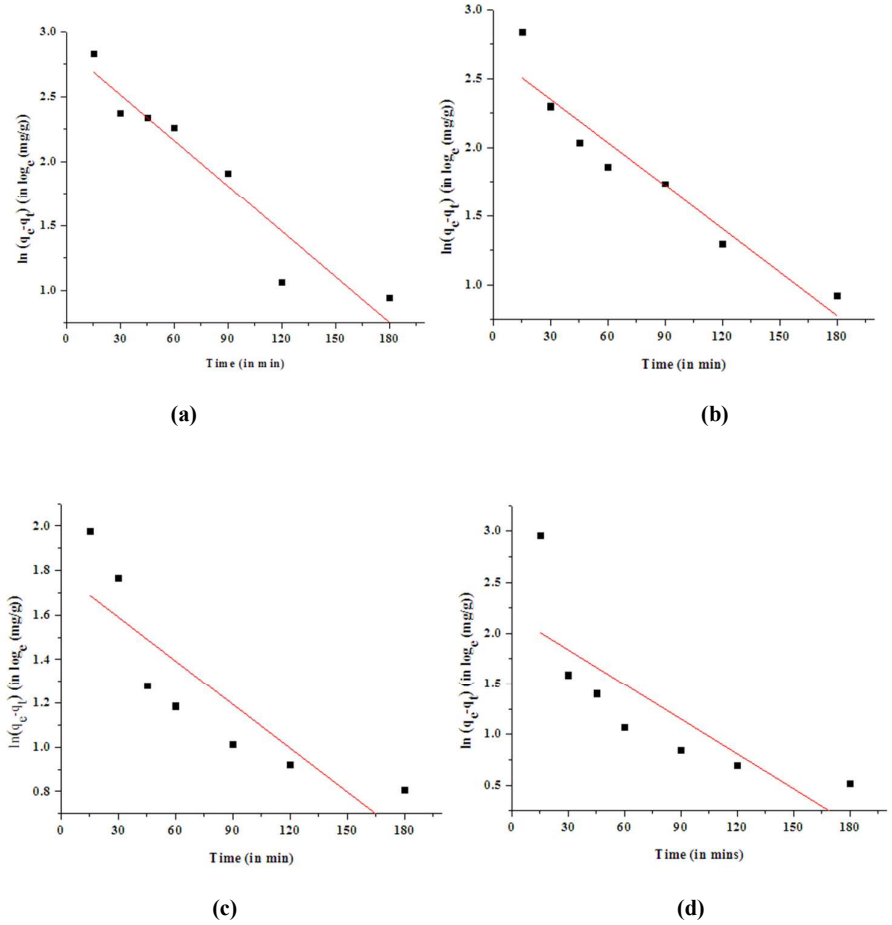

Figure 6: Pseudo first order kinetics curve fitting for the sorption mechanism by particles prepared at (a) 0°C (b) RT (25°C) (c) 50°C (d) 70°C

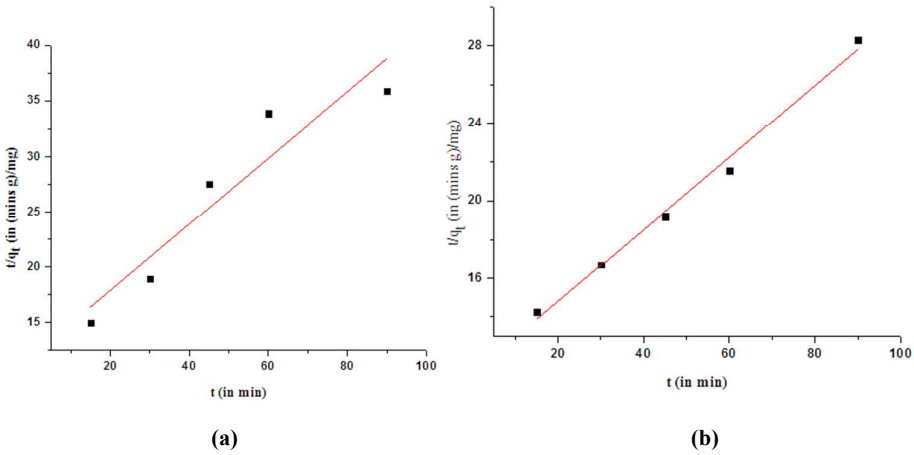

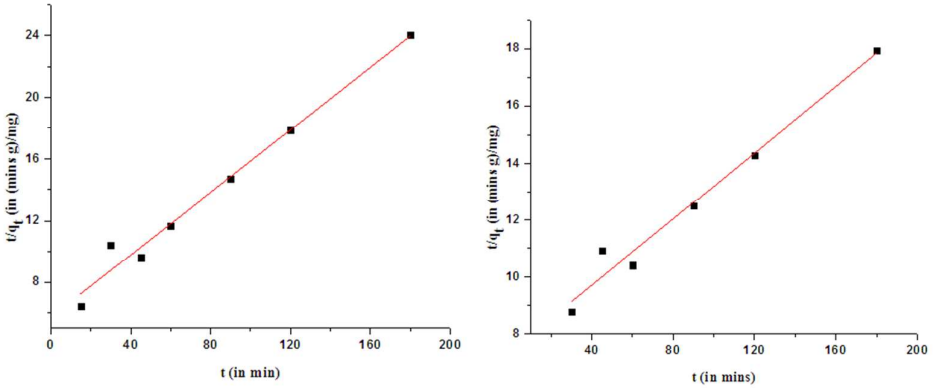

(c) (d)

Figure 7: Pseudo second order kinetics curve fitting for the sorption mechanism by particles prepared at (a) 0°C (b) RT (25°C) (c) 50°C (d) 70°C

Adsorption isotherms of Cr(VI) by pure Ni_2O_3 nanoparticles

Isotherm study being an important tool to analyse the adsorption capacity of the adsorbant indicates the distribution of adsorbed molecules between the solid and the liquid phase when the adsorption reaches equilibrium. To understand the adsorption behaviour of the adsorbant, two isotherm models were tested viz. Freundlich and Langmuir isotherms.[31,32]The Freundlich isotherm is expressed as follows:[31]

$$\ln q_e = \ln k_f + \frac{1}{n} \ln C_e \qquad (6)$$

It is considered that the particle surface is heterogeneous that is expressed by the degree of heterogeneity 'n' in the equation (6) The Freundlich plots for adsorption of Cr(VI) by pure Ni_2O_3 nanocrystals are presented in Figure 8. The value of the Freundlich constant 'k_f' and heterogeneity constant 'n', obtained from $\ln q_e$ vs. $\ln C_e$plot, are listed in Table - 4.

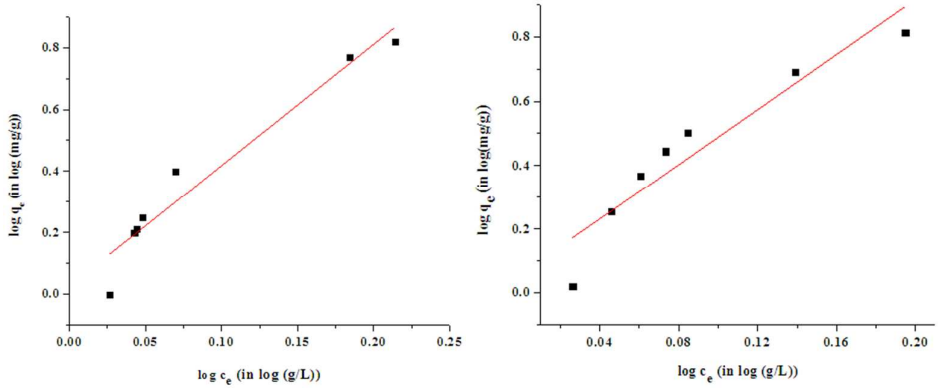

(a) (b)

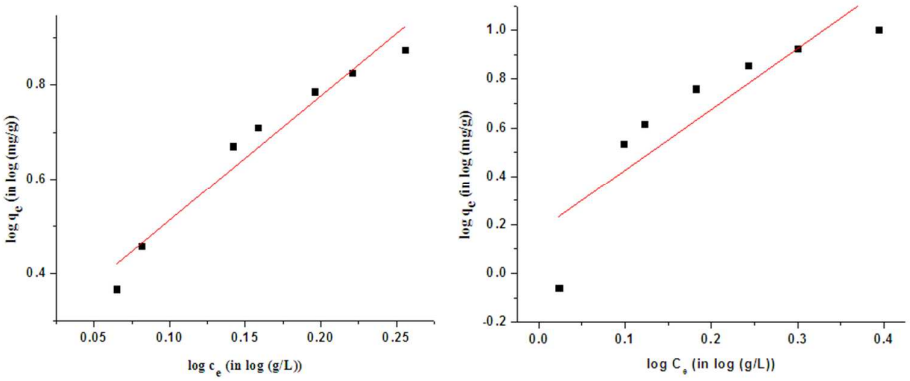

(c) (d)

Figure 8: Freundlich isotherm plots for the sorption mechanism by particles prepared at (a) 0°C (b) RT (25°C) (c) 50°C (d) 70°C

The Langmuir isotherm that has been developed on the basis of one site occupancy by one pollutant species on the homogenous surface of the adsorbant is expressed by the following equation:

$$\frac{C_e}{q_e} = \frac{1}{bQ_m} + \frac{C_e}{Q_m} \quad (7)$$

On simplifying the above relation, the following linear relation is obtained.

$$\frac{1}{q_e} = \frac{1}{bq_mC_e} + \frac{1}{q_m} \quad (8)$$

Figure 9 shows the Langmuir plots for the pure Ni_2O_3 nanoparticles. On plotting $1/q_e$ vs. $1/C_e$curves, Langmuir binding constants (b) and maximum adsorption (q_m)are calculated (tabulated in Table - 4).

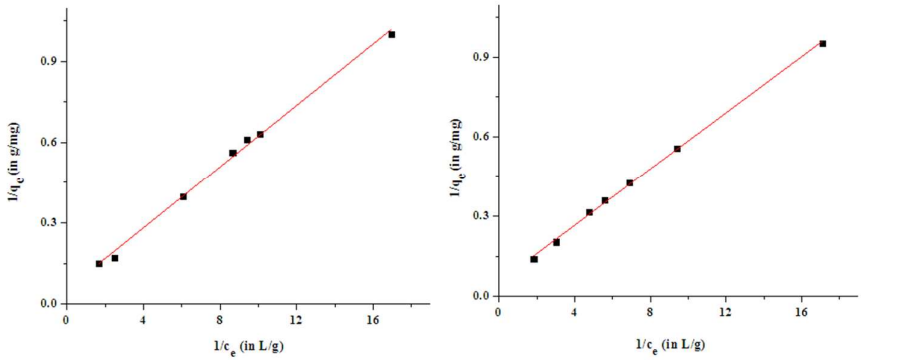

(a) (b)

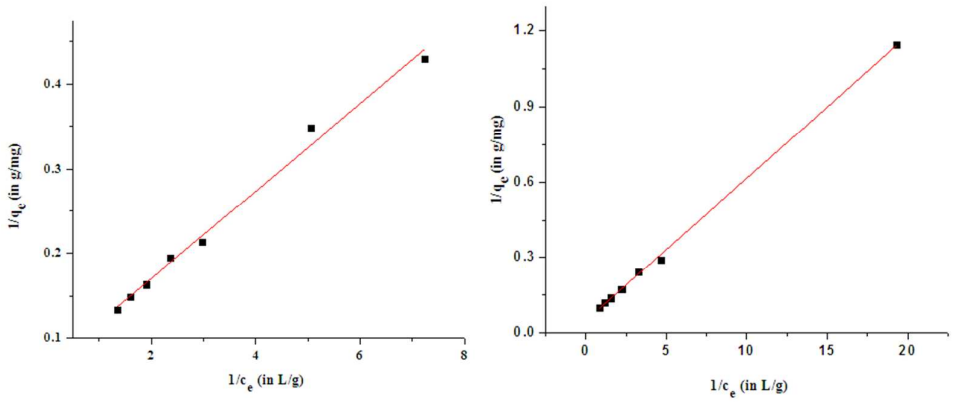

(c) (d)

Figure 9: Langmuir isotherm plots for the sorption mechanism by particles prepared at (a) 0°C (b) RT (25°C) (c) 50°C (d) 70°C

High value of r^2 signifies that the Langmuir isotherm fits well with the Cr(VI) adsorption data compare to Freundlich isotherm. From the value of q_m, it is observed that the binding constant is least for the particles prepared at 70°C. This explains the initial adsorption of Cr(VI) for the first 15 minutes when the adsorption rate is lowest for the particles at 70°C as noticed from Figure 4. Moreover, from Table 2, it is noticed that the spontaneity of the reaction for particles prepared at 70°C is the least. However, for particles having smaller size, the effective area for adsorption is less. As the particle size increases, more and more active adsorption sites are available. As a result, more number of Cr(VI) can be adsorbed in a single layer. As the adsorption follows Langmuir isotherm, it forms a monolayer of the pollutant species surrounding the nanoparticle. In such a case, if there is a tendency of formation of a second layer, the Cr(VI) ions of the second layer is repelled by the already existing layer. Therefore, the adsorption in this case is proportional to the surface exposed for adsorption. Hence, the particle having the highest size possesses highest adsorption ability.

The Freundlich isotherm results also show that the degree of surface heterogeneity of the particles prepared at 70°C is the most. This means that these particles have got more heterogeneous sites which act as additional active sites for Cr(VI) ion adsorption. Thus, this model also supports the particles prepared at 70°C to be the highest adsorber though they are the largest particle size having lowest spontaneity of reaction. The comparison of the adsorption capacity of Ni_2O_3 with other materials has been thoroughly discussed in the ESI.

Table 3: Adsorption isotherm parameters obtained for pure Ni_2O_3 nanoparticles prepared at different temperatures

Synthesis temperature (in °C)	Freundlich Isotherm			Langmuir Isotherm		
	n (Degree of Heterogeneity)	k_f (Freundlich Constant)	r^2	b (in L mg^{-1})	q_m (in mg g^{-1})	r^2
0°C	0.255	1.026	0.935	0.964	18.519	0.996
25°C (RT)	0.234	1.063	0.872	1.000	18.868	0.999
50°C	0.378	1.282	0.945	1.314	18.925	0.989
70°C	0.400	1.192	0.745	0.875	20.408	0.999

It has been observed from above discussion that the adsorption and the associated degradation are significantly dependent on the particle size. Therefore, in order to get more insight into the above mentioned mechanism, we have thermodynamically computed the free energy (G_0) of the sorption reaction using the following relations:[32,33]

$$\ln k_d = \frac{-G_0}{RT} \quad (9)$$

and $$k_d = \frac{Q_e}{C_e} \quad (10)$$

where, 'k_d', 'T' and 'R' are the distribution coefficient, temperature (in K) and universal gas constant (8.314 J $mole^{-1}K^{-1}$) respectively. Therefore, a correlation has been drawn between the particle size and distribution coefficient to relate enthalpy, entropy and Gibb's free energy of the adsorption process on the basis of formation of a homogeneous single layer of Cr(VI) ion around the particle. Considering radius of a single particle to be 'r', the effective surfaces for adsorption increase with decrease in size. As adsorption is a surface phenomenon, the volume atoms and their contribution can be neglected. Thus, surface available for adsorption is $4\pi r^2$. Therefore, from the results of adsorption, it can be considered that amount of Cr(VI) adsorbed in directly proportional to the adsorbant surface and may be written as: $Q_e \alpha r^2$, which in turn implies $Q_e = s.r^2$, where 's' is the surface constant that is equal to 4π x 'number of effective surface per molecule of adsorbant'. The number of effective surface per molecule is a property of a molecule in any polar solvent and hence, it is constant for a particular molecule. Again, adsorption of any ionic species on the surface of the nanoparticles is supposed to be proportional to the

potential corresponding to surface charge in the absence any shielding effect (Q_e α ξ). In the presence of any electrical double layer that causes shielding, Q_e would be inversely proportional to σ ($Q_e \alpha \frac{1}{\sigma}$).[33] However, for smaller particles, the shielding effect that forms an electrical double layer which effectively prevents adsorption. Therefore using equations (9) and (10), it may be written,

$$\ln k_d = (\ln s - \ln C_e - \ln \sigma + \ln \xi) + 2 \ln r \quad (11)$$

$$\ln k_d = (\ln \frac{s.\xi}{\sigma.C_e}) + 2 \ln r \quad (12)$$

This is essentially a linear relation. Thus, on plotting the straight line curve of $\ln k_d$ vs.lnr, the surface constant 's' and in turn the number of active surfaces available for adsorption can be calculated. The plot is illustrated in figure 10.

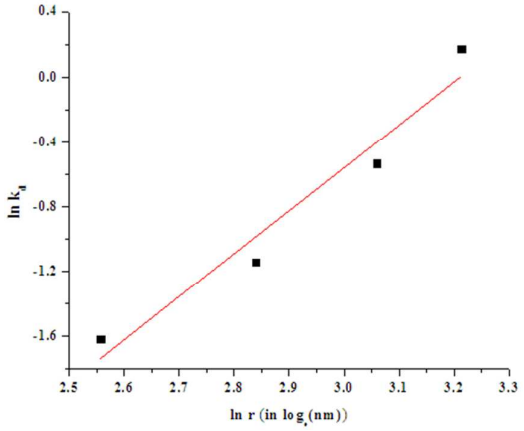

Figure 10: Relation between ln k_d and ln r

Now, from the intercept, $\ln k_d^0 = \ln(\frac{s.\xi}{\sigma}) - \ln C_e$ curve, where k_d^0 may be considered as the distribution coefficient for a particle of unit dimension, it is possible to calculate $\frac{s}{\sigma}$ that denotes the effective adsorption taking place per unit weight of the adsorbant per unit shielding potential which obstructs the effective adsorptionusing the following equation,

$$\frac{s}{\sigma} = \frac{k_d^0.C_e}{\xi_0} \quad (13)$$

Again, using (9) and (11), Gibb's Free Energy 'G_0' (positivity or negativity will depend on values of 'r','s' and 'C_e' and hence is considered without the negative sign) can be calculated as follows:

$$G_0 = 2RT \ln r + RT (\ln(\frac{s.\xi}{\sigma}) - \ln C_e) \quad (14)$$

Table 5 enlists the thermodynamic parameters calculated from the above results. It is observed that reaction spontaneity decreases as the particle size increases. Thus, it can be concluded from the results that smaller particles undergo a more spontaneous reaction as compared to the larger particles.

Table 5: Thermodynamic and surface parameters of adsorption reaction by pure Ni_2O_3 nanoparticles

Radius (in nm)	$\frac{s}{\sigma}$ (in mg g^{-1} mV^{-1})	G_0 (in Joules/mole)
12.9	7.68 x 10^{-5}	-8457.30
17.1	1.09 x 10^{-4}	-7060.69
21.3	8.66 x 10^{-5}	-5972.40
24.85	8.73 x 10^{-5}	-5208.56

From the above result, it can be seen that adsorption coefficient is highest for the particles prepared at room temperature. This can be attributed to the extent of heterogeneity of the room temperature particles. However, due to the screening effect of the H^+ ions, the effective adsorption decreases in case of the smaller particles. Thus, the 70^{o}C synthesized particles which are largest in size, has the highest effective adsorption.

Conclusions

Pure Ni_2O_3 nanoparticles are prepared by a mild, environment friendly, room temperature process. Particles of four different sizes are prepared varying from ~25.8 nm to 49.7 nm by varying the synthesis temperature. The activation energy of formation of the Ni_2O_3 nanoparticles is calculated to be ~75.49 meV. A relation between particle size and Gibb's free energy have been formulated to calculate the degree of spontaneity and number of active adsorption sites per unit area for particles with different particle size. The prepared particles are found to possess excellent Cr(VI) adsorption capacity adsorbing about ~60% Cr(VI) in 3 hours from its aqueous solution. Thus, this material has a potential to replace the conventional adsorbents used commercially which has lower time efficiency of heavy metal removal. The material thus possesses huge environment friendly impact that will improve the hydrosphere condition drastically throughout the globe thereby addressing several major global threats possessed by the industries.

Acknowledgements

The authors (SB& SH) wish to thank the University Grant Commission, the Govt. of India for University with Potential for Excellence (UPE - II) scheme.

References

1. R. Hana, W. Zoua, Z. Zhang, J. Shi, J. Yang, Journal of Hazardous Materials B, 2006, **137**, 384.
2. A. Zhitkovich, Chem. Res. Toxicol. 2011, **24**, 1617.
3. B. Qiu, H. Gu, X. Yan, J. Guo, Y. Wang, D. Sun, Q. Wang, M. Khan, X. Zhang, B.L. Weeks, D.P. Young, Z. Guo, S. Wei, 2014, **2**, 17454.
4. H. Gu, S.B. Rapole, J. Sharma, Y. Huang, D. Cao, H.A. Colorado, Z. Luo, N. Haldolaarachchige, D.P. Young, B. Walters, S. Wei, Z. Guo, RSC Adv. 2012, **2**, 11007.
5. B. Qiu, C. Xu, D. Sun, H. Wei, X. Zhang, J. Guo, Q. Wang, D. Rutman, Z. Guo, S. Wei, RSC Adv., 2014, **4**, 29855.
6. S. Mellah, S. Chegrouche, M. Barkat, Hydrometallurgy, 2007, **85,** 163.
7. H. Singh, S.L. Mishra, R. Vijayalakshmi, Hydrometallurgy, 2004, **73**, 63.
8. V.P. Ravi, R.V.Jasra, T.S.G. Bhat, J. Chem. Technol. Biotechnol. 1998, **71**, 173.
9. J.P. Chen, S. Wu, J Chem Technol Biotechnol, 2000,**75**, 791.
10. T. Yao, T. Cui, J. Wu, Q. Chen, S. Lu, K. Sun,Polym. Chem., 2011, **2**, 2893.
11. R. Ansari, N.K. Fahim, Reactive & Functional Polymers, 2007,**67**, 367.
12. S. Bettini, R. Pagano, L. Valli, G. Giancane, Nanoscale, 2014, **6**, 10113.
13. M.E. Grass, Y.Yue, S.E. Habas, R.M. Rioux, C.I. Teall, P. Yang, G.A. Somorjai, J. Phys. Chem. C 2008, **112**, 4797.
14. L. Tan, J. Wang, Q. Liu, Y. Sun, X. Jing, L. Liu, J. Liu, D. Song, NewJ.Chem., 2015, **39**, 868.
15. J. Quinton, L. Thomsen, P. Dastoor, 1997, **25**, 931.
16. R.C. Vaishya, S.K. Gupta, J. Chem Technol Biotechnol, 2002,**78**, 73(online).
17. C.Tiffreau, J.Lutzenkirchen, P.Behra, 1995, **172**, 82.

18. J. M. Tarascon and M. Armand, Nature, 2001, **414**, 359.
19. S.H. Park, S.H. Kang, C.S. Johnson, K. Amine, M.M. Thackeray, Electrochemistry Communications, 2007,**9**, 262.
20. L. Wöhler,O. Balz, Z. Elektrochem., 1921, **27**, 415.
21. H. Baubigny, Compt Mend., 1905, **87**. 1082, 1878 ;141. 1232.
22. R.W. Cairns, E. Ott, J. Am. Chem. Soc.,1933, **55**, 527.
23. T. Yao, T. Cui, J. Wu,Q. Chen, S. Lu, K. Sun, Polym. Chem., 2011, **2**, 2893.
24. B.D. Cullity, "Elements of X-Ray Diffraction", 1956, Addison-Wiley Publishing Company Inc., **56-10137**.
25. S. J. Iyengar, M. Joy, C. Ghosh, S. Dey, R. K. Kotnala, S. Ghosh, RSC Adv., 2014, **DOI: 10.1039/C4RA11283K**.
26. Q. Yang, G. Chen, J. Zhang, H. Li, RSC Adv., 2015, **5**, 25541.
27. A. Kamari, W.S.W. Ngah, M.Y. Chong, M.L. Cheah, Desalination, 2009, **249**, 1180.
28. I. Langmuir, J. Am. Chem. Soc., 1918, **40**, 1361.
29. J. X. Li, Z. Q. Guo, S. W. Zhang, X. K. Wang, Chem. Eng. J., 2011, **172**, 892.
30. H. M. F. Freundlich, J. Phys. Chem., 1906, **57**, 385.
31. W.T. Tsai, Y.M. Chang, C.W. Lai, C.C. Lo, J. Colloid Interface Sci., 2005, **289**, 333.
32. M. Sprynskyy, B. Buszewski, A. P. Terzyk, J. Namiesnik, J. Colloid Interface Sci., 2006, **304**, 21.
33. D.E. Yates, S. Levine, T.W. Healy, Journal of the Chemical Society Faraday Transactions, 1974, **1(70)**.

Supporting information

Synthesis of pure nickel(III) oxide nanoparticles at room temperature for Cr(VI) ion removal

Sayan Dey[(a)], Swarupananda Bhattacharjee[(a)], Mahua Ghosh Chaudhuri[(a)], Raj Shekhar Bose[(b)], Suman Halder[(c)] and Chandan Kr. Ghosh[(a)]

[(a)]School of Materials Science and Nanotechnology, Jadavpur University, Kolkata-700032, India
[(b)]School of Environmental Studies, Jadavpur University, Kolkata – 700032, India.
[(c)]Department of Pharmaceutical Technology, Jadavpur University, Kolkata – 700032, India
* Corresponding author's e-mail ID: chandu_ju@yahoo.co.in

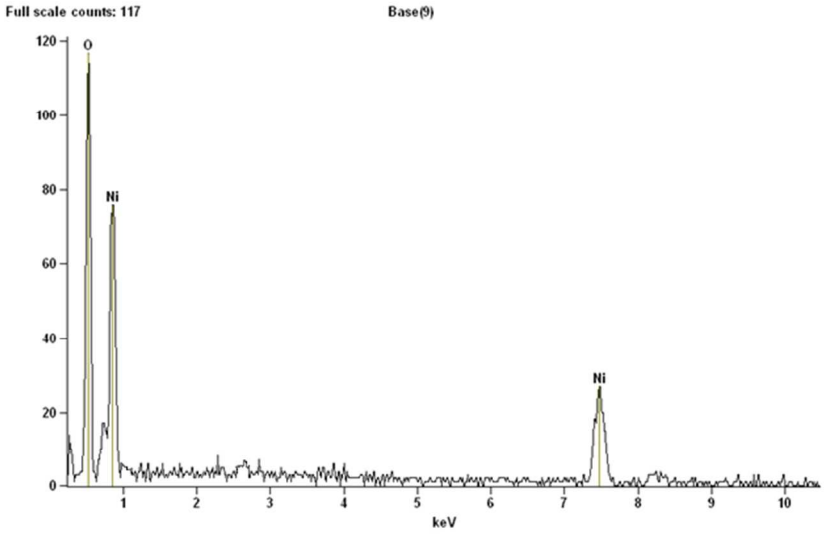

Figure S -1: EDAX micrograph showing elemental composition of pure Ni_2O_3 nanoparticles

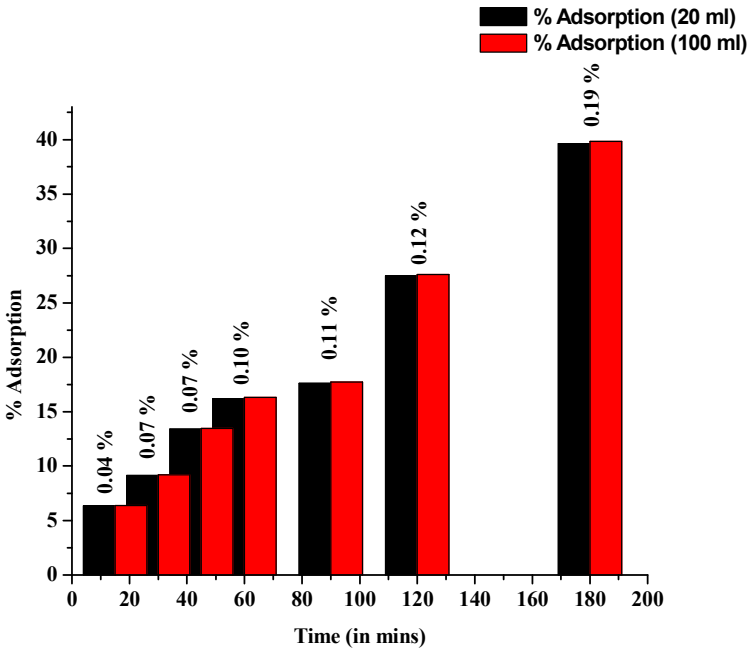

Figure S - 2: Variation of adsorption (pH = 6, Ni_2O_3 0.02 gm, speed 600 rpm) with respect to time for 2 ml stock solution (black bar) and 100 ml stock solution (red bar). Numeric represents the difference in adsorption percentage.

In order to examine human error introduced during preparation of stock solution, adsorptions were carried out using two different stock solutions (20 ml and 100 ml) keeping the concentrations fixed (0.02 gm per ml, similar to 0.4 gm in 20 ml, shown in Figure S - 2). Here we have measured the adsorption using Ni_2O_3 nanoparticles synthesized at room temperature (RT, 25°C). The maximum difference is found to be 0.19% in the case of 3 hours of stirring time.

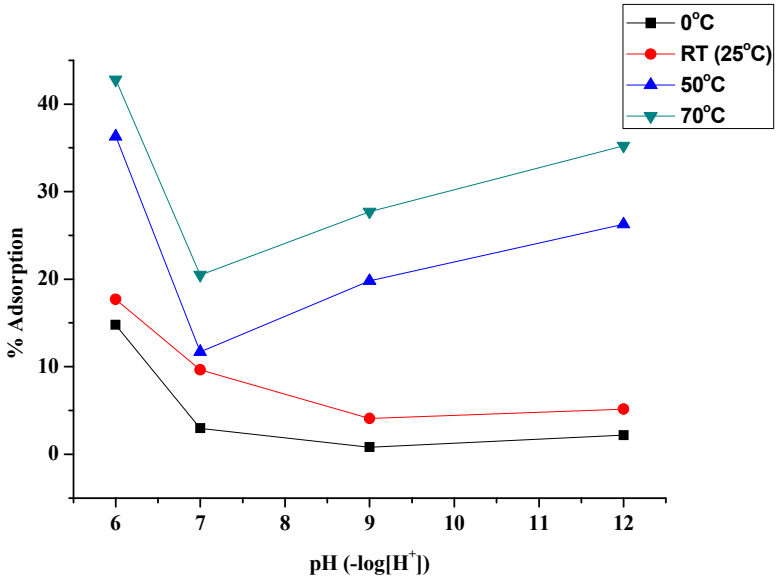

Figure S - 3: Variation of adsorption with respect to pH of the solution (0.4gm $K_2Cr_2O_7$ in 20 ml, 0.02 gm Ni_2O_3, pH = 6, time 1.5 hours, 600 rpm).

The pH value of the solution significantly affects the forms of Cr(VI) and ionic state of the Ni_2O_3. In this present work, the effect pH on Cr(VI) adsorption has been investigated over a wide range of pH ranging from 3 to 12. In the acidic pH (< 3), Ni_2O_3 is found to be not stable; hence adsorption of the synthesized nanoparticles has been presented in the pH range 6 to 12 in Figure S -3. From figure it may be concluded that the adsorption is maximum at pH = 6. Interestingly, adsorption is found to be decreased for all particles in the pH range between 6 and 7. At higher pH (> 7), adsorption is noticed to be increased for nanoparticles having higher size (synthesized at 50^0C and 75^0C), whereas it remains almost unchanged for others two nanoparticles having smaller size (synthesized at freezing temperature and 25^0C). The initial reduction of the adsorption (below pH = 7) may be attributed to the predominant electrostatic repulsion between negatively charged Ni_2O_3 surface and negatively charged OH^- of surrounded Cr(VI). The higher sized particles have less surface charge (as it is examined by zeta potential measurement), so their repulsion gets reduced, as a result their Cr(VI) adsorption capability is found to be enhanced compare to lower sized particles.

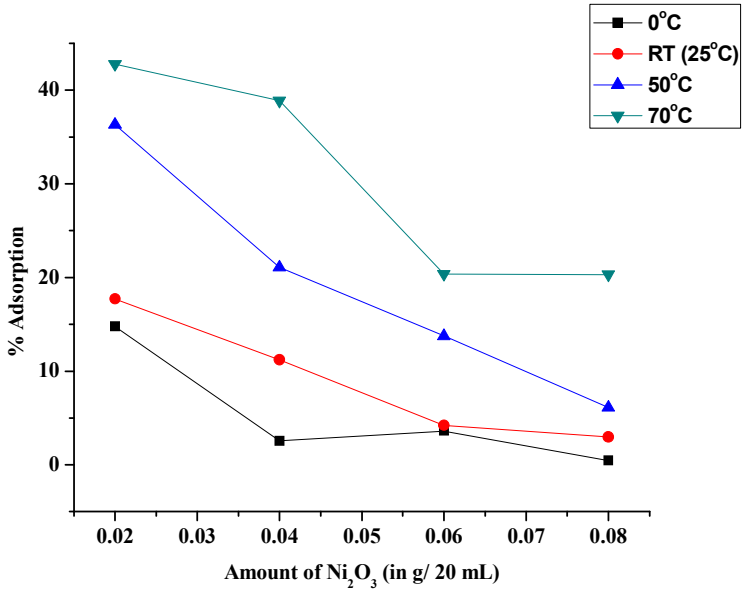

Figure S - 4: Variation of Cr(VI) adsorption with respect to adsorbent dose (0.4gm $K_2Cr_2O_7$ in 20 ml, pH = 6, 1.5 hrs, 600 rpm).

The effect of adsorbent dose on Cr(VI) removal process was examined at room temperature for four different sized Ni_2O_3 nanoparticles and the variation is presented in Figure S - 4. It has been clearly observed from figure that Cr(VI) removal efficiency decreases with increasing adsorbent dose and it found to be maximum at 0.02 gm of Cr(VI). Similar type of variation was observed by Chen et al.[1] As we increase adsorbent dose, some agglomeration of the nanoparticles is observed. Hence the lowering of the removal capacity may be attributed to the deposited agglomerated nanoparticles. We set the adsorbent dose 0.02 gm in 20 ml for all other measurement.

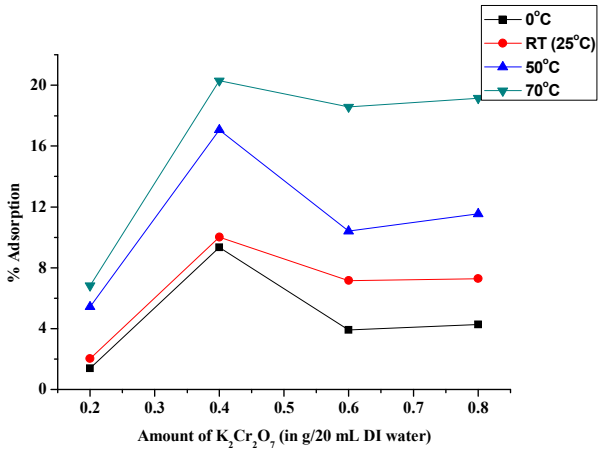

Figure S - 5: Adsorbate variation (pH 6, $Ni_2O_3$0.02 gm in 20 ml, 600 rpm, time 1.5 hours).

Initial concentration of Cr(VI) was varied after taking different amount of $K_2Cr_2O_7$ viz. 0.2, 0.4, 0.6 and 0.8 gm in 20 ml of solution (shown in Figure S - 5). During this measurement, pH and amount of Ni_2O_3 were kept fixed 6.0 and 0.40 gm respectively. It is observed from figure that the maximum adsorption takes place corresponding to 0.40 gm of $K_2Cr_2O_7$ in 20ml water. Hence, we have chosen this concentration of $K_2Cr_2O_7$ for all other measurements.

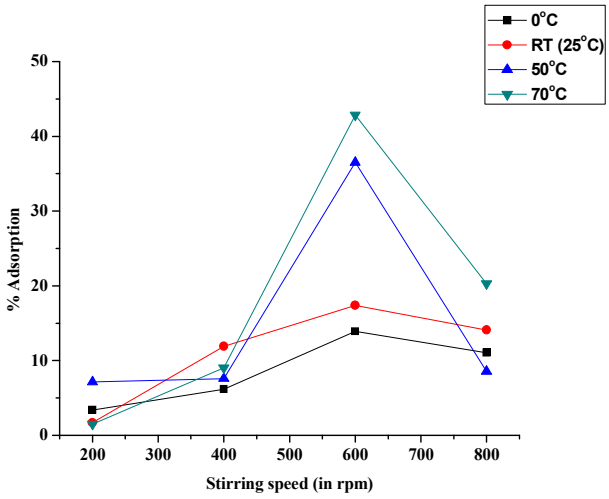

Figure S- 6: Variation of Cr(VI) adsorption with speed of the shaker.

Figure S –6: represents the variation of Cr(VI) removal capacity as a function shaker speed. During this experiment, we kept pH = 6, the amount of Ni_2O_3 was taken 0.02 gm. From the figure, it may be concluded that adsorption is maximum at 600 rpm. So we set this shaking speed for all other measurements.

We have compared Cr(VI) capacity of our synthesized sample with adsorption capacity of some other materials (shown in Table T – 1 in ESI). It is interesting to note that our synthesized Ni_2O_3 nanoparticles possess higher adsorption capacity compare to carbon coated magnetic nanoparticles, α-Fe_2O_3, CeO_2 etc., but has less adsorption capacity than activated carbon, aluminium – magnesium mixed hydroxide. It is worthy to state that the mechanism involved Cr(VI) in the case of aluminium – magnesium mixed hydroxide is the ion exchange, not the adsorption process. Therefore fundamentally it involves different mechanism. Activated carbon though relies on adsorption possesses higher adsorption capability due to their light mass. Therefore, we may conclude that our synthesized nanoparticles have higher removal capacity of Cr(VI).

Table T – 1: Comparison of adsorption process with other materials

Material used	Adsorption (mg/g)	Reference
Carbon coated magnetic nanoparticles	1.52	2
Agriculture waste biomass	0.28 – 0.82	3
Graphene nanocomposites	1.03	4
Commercial α-Fe2O3	0.68	5
Commercial CeO_2	0.37	6
3D flower-like CeO_2	5.9	6
Aluminium – magnesium mixed hydroxide	105	7
Activated carbon	112	8
Polyaniline coated carbon fiber	18.1	9
Ni_2O_3 nanoparticles	20.408	Present work

In recent time, some new materials like rosin-based biochar - α-Fe_2O_3 nanocomposites[10], zinc – biochar nanocomposites[11], magnetic mesoporous carbon – polyaniline composites[12], tartaric acid modified Pleurotus ostreatus[13] have been developed by researchers and they are found to have much higher Cr(VI) adsorption capacity. Importantly, their maximum adsorptions are found to be in the range of either basic pH (~ 9) or acidic pH (~ 2). But, here we obtained the maximum adsorption capacity of our synthesized sample very close to neutral pH (~ 6). So to remove Cr(VI) from aqueous solution having pH close neutral, our synthesized sample may be helpful.

Standard deviation of the measurements was calculated using the following relation for sample synthesized at room temperature as a function time (15, 30, 45, 60, 90, 120 and 180 minutes),

$$\text{Standard deviation} = \sqrt{\frac{1}{5}\sum_{i=1}^{5}(R_i - R_{av})^2}$$

Where, R_i and R_{av} represent the adsorption percentage for each measurement and the average adsorption respectively. The variation of standard deviation with respect to time is presented in Figure S - 7.

Accuracy of the used system
(a) UV-Vis spectrophotometer (JASCO, V- 650)
± 0.002 Abs

(b) Digital balance
± 0.001 g

(c) Measuring cylinder
± 0.2 ml

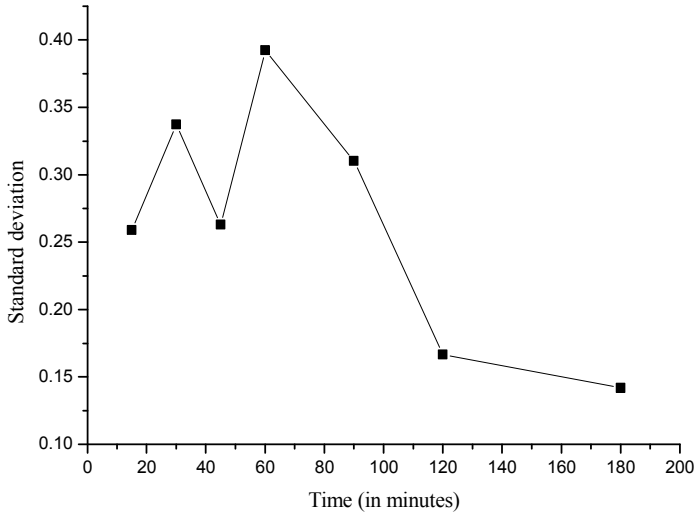

Figure S – 7: Variation of standard deviation of the percentage of adsorption with respect to time.

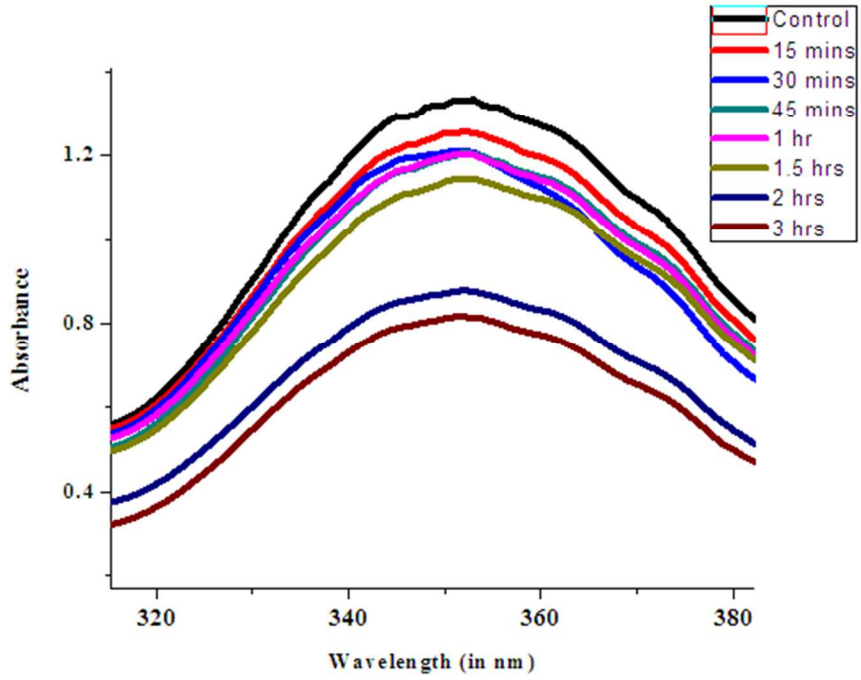

Figure S -8: UV spectrum of Cr (VI) adsorption by particles synthesized at 0^{o}C.

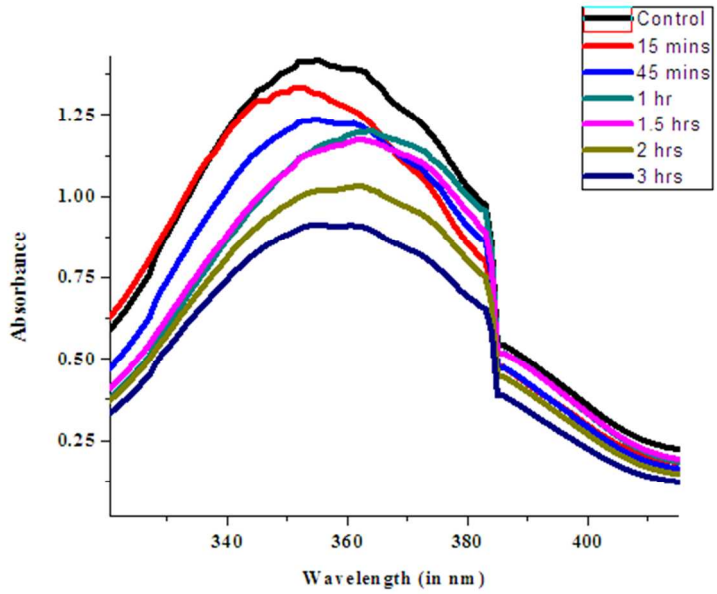

Figure S - 9: UV spectrum of Cr (VI) adsorption by particles synthesized at room temperature (25^{o}C).

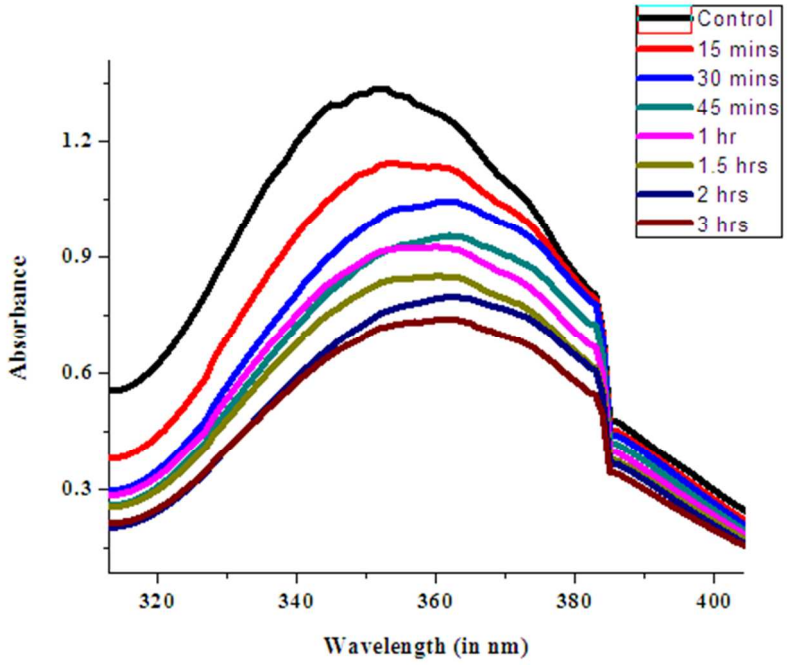

Figure S – 10: UV spectrum of Cr (VI) adsorption by particles synthesized at 50^{o}C.

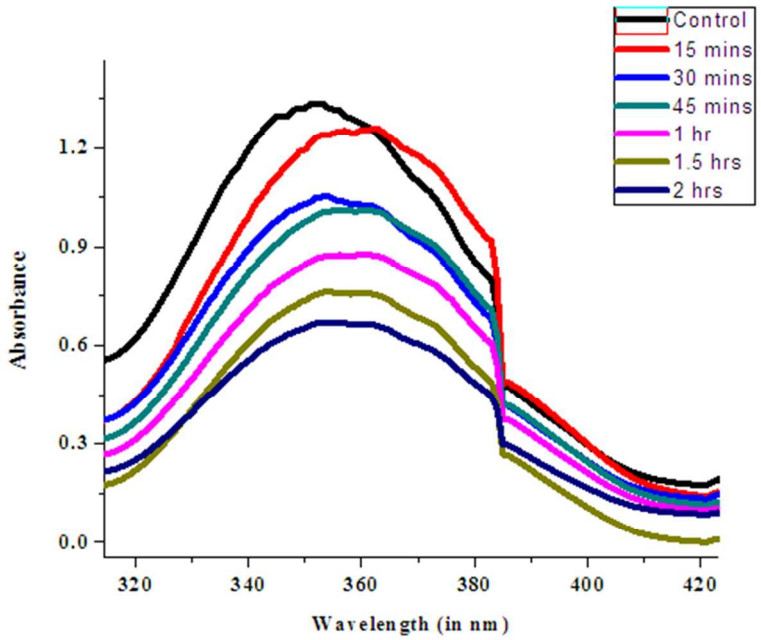

Figure S - 11: UV spectrum of Cr (VI) adsorption by particles synthesized at 70°C.

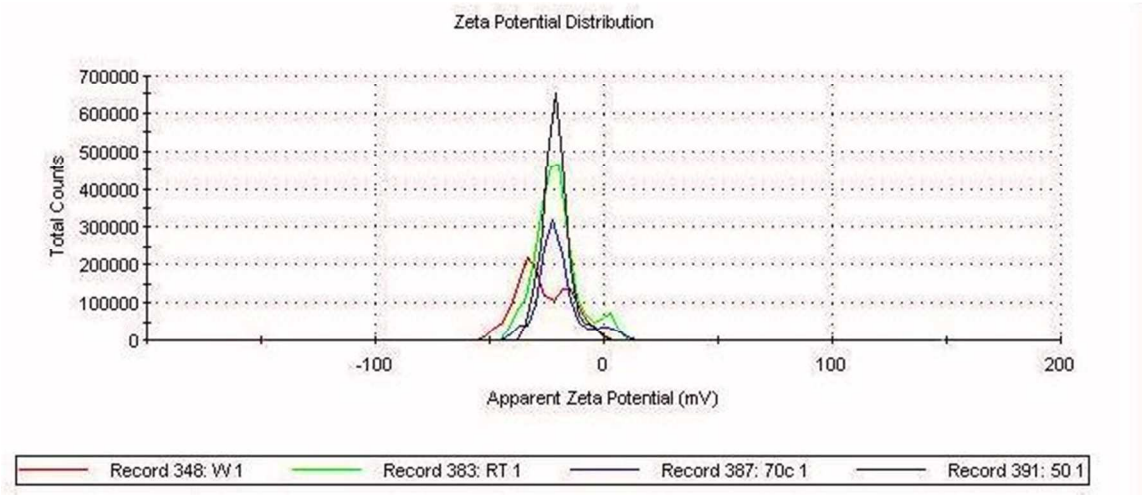

Figure S – 12: Comparison of the Zeta potentials of Ni_2O_3 nanoparticles of different size.

References:

1. Y. Chen, H. Xu, S. Wang and L. Kang, RSC Adv. 2014, **4**, 17805.
2. J. Zhu, H. Gu, S.B. Rapole, Z. Luo, S. Pallavkar, N. Haldolaarachchige, T. J. Benson, T. C. Ho, J. Hopper, D. P. Young, S. Wei and Z. Guo, RSC Adv., 2012, **2**, 4844–4856.
3. U. K. Garg, M. P. Kaur, V. K. Garg and D. Sud, J. Hazard. Mater., 2007, **140**, 60–68.
4. J. Zhu, S. Wei, H. Gu, S. B. Rapole, Q. Wang, Z. Luo, N. Haldolaarachchige, D. P. Young and Z. Guo, Environ. Sci. Technol., 2012, **46**, 977–985.
5. L. S. Zhong, J. S. Hu, H. P. Liang, A. M. Cao, W. G. Song and L. J. Wan, Adv. Mater., 2006, **18**, 2426–2431.
6. L.S. Zhong, J.-S. Hu, A.-M. Cao, Q. Liu, W.-G. Song and L.-J. Wan, Chem. Mater., 2007, **19**, 1648–1655.
7. Y. Li, B. Gao, T. Wu, D. Sun, X. Li, B. Wang and F. Lu, Water Res., 2009, **43**, 3067–3075.
8. A. El-Sikaily, A. E. Nemr, A. Khaled, O. Abdelwehab, J. Hazard. Mater., 2007, **148**, 216–228.
9. B. Qiu, C. Xu, D. Sun, H. Wei, X. Zhang, J. Guo, Q. Wang, D. Rutman, Z. Guo, S. Wei, RSC Adv.,2014, **4**, 29855.
10. Z. H. Ruan, J. H. Wu, J. F. Huang, Z.T. Lin, Y. F. Li, Y. L. Liu, P. Y. Cao, Y. P. Fang, J. Xie, G. B. Jiang, J. Mater. Chem. A, 2015, **3**, 4595.
11. C. Gan, Y. Liu, X. Tan, S. Wang, G. Zeng, B. Zheng, T. Li, Z. Jiang, W. Liu, RSC Adv., 2015, **5**, 35107.
12. G. Yang, L. Tang, Y. Cai, G. Zeng, P. Guo, G. Chen, Y. Zhou, J. Tang, J. Chen, W. Xiong, RSC Adv.,2014, **4**, 58362.
13. T. Y. Lin, D. H. Chen, RSC Adv., 2015, **5**, 24009.